Microstructures

Research Article

Open Access

Check for updates

180° head-to-head flat domain walls in single crystal BiFeO₃

Wanbing Ge[1], Richard Beanland[1] ⓘD, Marin Alexe[1], Quentin Ramasse[2], Ana M. Sanchez[1]

[1]Department of Physics, University of Warwick, Coventry CV4 7AL, UK.
[2]SuperSTEM Laboratory, SciTech Daresbury, Keckwick Lane, Warrington WA4 4AD, UK.

Correspondence to: Prof. Richard Beanland, Department of Physics, University of Warwick, Coventry CV4 7AL, UK. E-mail: R.Beanland@warwick.ac.uk

Abstract

We investigate flux-grown BiFeO₃ crystals using transmission electron microscopy (TEM). This material has an intriguing ferroelectric structure of domain walls with a period of approximately 100 nm, alternating between flat and sawtooth morphologies. We show that all domain walls are of 180° type and that the flat walls, lying on (112) planes, are reconstructed with an excess of Fe and a deficiency of Bi. This reconstruction is similar to that observed in several previous studies of deposited layers of BiFeO₃. The negative charge of the reconstructed layer induces head-to-head polarisation in the surrounding material and a rigid-body shift of one domain relative to the other. These characteristics pin the flat 180° domain walls and determine the domain structure of the material. Sawtooth 180° domain walls provide the necessary reversal of polarisation between flat walls. The high density of immobile domain walls suppresses the ferroelectric properties of the material, highlighting the need for careful control of growth conditions.

Keywords: Bismuth ferrite, ferroelectric domains, 180° domain walls, reconstructed domain walls

INTRODUCTION

BiFeO₃ is arguably the most investigated multiferroic material[1-3], simultaneously showing ferroelectric, antiferromagnetic, and ferroelastic order at room temperature[4]. The coupling of ferroelectric and ferromagnetic properties makes it ideal for the promising application of mutual control of electrical and

magnetic order in multiferroic devices[5,6].

BiFeO$_3$ has a rhombohedral structure (space group *R3c*) below its Curie temperature T_c = 1,100 K[4], with a pseudocubic lattice parameter of 3.965 Å and rhombohedral angle 89.4° (pseudocubic indexing is used throughout this paper). Its spontaneous ferroelectric polarisation (**P**$_s$) has a magnitude P_s approximately 100 µC cm^{-2} along [111] and mostly arises from the displacement of Bi ions relative to their surrounding FeO$_6$ cages[7]. Oxygen octahedra are tilted antiphase around the three-fold [111] axis by 10°-14° ($a^-a^-a^-$ in Glazer notation[8]). The formation of domains in BiFeO$_3$, similar to other ferroelectric materials, occurs to minimise the total energy, comprised of electrostatic, depolarisation, and elastic components[9]. Depending on the angle ϕ between **P**$_s$ of adjacent domains, the meeting of these domains at domain walls can result in either purely ferroelectric (ϕ = 180°) or ferroelectric-ferroelastic (ϕ = 71° or 109°). The orientation or habit plane of domain walls has been of great interest as it provides insight into the competing energy components[10-13] and determines functional properties[14,15].

The batch of flux-grown single-crystals of BiFeO$_3$ investigated in this study have been subject to several previous investigations[16,17], all of which have revealed a dense array of parallel domain walls seen in piezoresponse force microscopy (PFM) and conventional transmission electron microscopy (TEM) as alternating sawtooth and flat bands of contrast [Figure 1]. The complex microdomain structure in these crystals is extremely stable, exhibiting no change upon observation, even in the thinnest specimens. Furthermore, no observable switching (or rapid back-switching into the pristine domain pattern) was found, even with 200 V applied to the surface with an AFM tip. The inability to access the functional properties of these high-quality single crystals is concerning and may have implications for the exploitation of BiFeO$_3$ in practical applications. Therefore, it is important to understand the nature and origin of this domain structure.

The first study of these crystals[16] showed the domain walls to be either 180°- or 109°-type and due to the high predicted energy of 180°-type domain walls, it was proposed that they were probably 109°-type. A second study[17] of the same batch of crystals using negative C_s high-resolution TEM imaging found a variety of domain wall types, including 71°-, 109°-, and 180°-type. Another recent study of similar material[18] confirms the sawtooth walls to be 180°-type but proposes that flat domain walls are 109°-type. In this article, along with its companion publication[19], we revisit the domain structure in this same batch of crystals using a combination of PFM, conventional TEM, convergent beam electron diffraction (CBED), atomic resolution scanning TEM (STEM), and electron energy loss spectroscopy (EELS). The high stability of the domains ensured there was no influence of specimen preparation on the structure. We find that there are only 180° domains in the crystal, i.e., all domain walls are 180°-type. The difficulties experienced in previous work may potentially be attributed to projection effects when the three-dimensional domain structure is observed in an electron-transparent foil. To overcome this, we use a focused ion beam (FIB) technique to prepare multiple sections with different orientations from the same region of the crystal. We describe the sawtooth domains in a companion article[19]; the focus of this article is on the flat 180° domain walls.

MATERIALS AND METHODS

BiFeO$_3$ single crystals were obtained from the same batch used in the studies of Berger *et al.*[16] and Jia *et al.*[17], who described growth conditions in detail. In brief, crystals were precipitated from a Fe$_2$O$_3$/Bi$_2$O$_3$/B$_2$O$_3$ flux cooled very slowly from 1,170 K to 875 K. Much of the growth took place below the paraelectric-ferroelectric phase transition at 1,098 K. The crystals were compact and had sizes of half to a few millimetres, with a top surface of four (*hhl*) facets, only a few degrees away from (001). For this study, several well-formed single crystals that had no contact with the crucible sidewalls were selected.
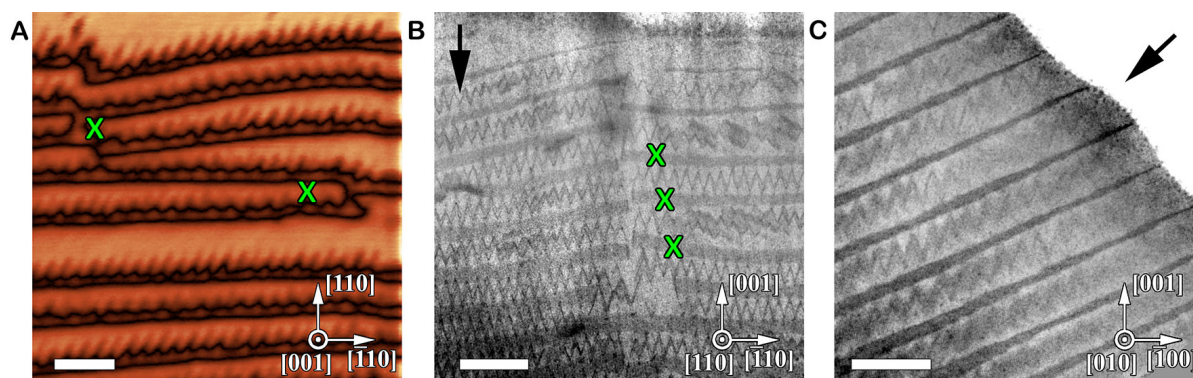
Figure 1. (A) PFM out-of-plane amplitude image of the sectioned and polished (001) surface of the $BiFeO_3$ crystal. (B) Low magnification BF-STEM image of a (110) FIB-prepared lamella. (C) Low magnification BF-STEM image of a (010) FIB-prepared lamella. Arrows in (B and C) point towards increasing thickness. Examples of continuity of domain walls, where a sawtooth wall changes direction and becomes a flat wall, are marked by x in (A and B). Scale bars are 100 nm.

For PFM measurements, a crystal was ground and polished to (001) using diamond lapping film of decreasing sizes to 0.1 μm, finishing with a dilute 0.04 μm colloidal silica solution. PFM measurements were conducted on a Bruker Dimension Icon AFM at a scan rate of 0.5 Hz using a Bruker OSCM-PT-R3 tip with Pt coating, along with a drive frequency of 254 kHz and a drive voltage of 2 V.

Specimens for TEM were prepared by lift-out on a Tescan Amber Ga⁺ FIB-SEM from a second crystal in its as-grown state, with (110), (010), and ($\bar{1}$10) orientations. Cutting and thinning were performed using an ion beam energy of 30 kV, with a final low-energy polish at 2 kV. The specimens were taken from a compact region on the crystal, and their orientations were verified by their relative position, selected area electron diffraction (SAED) patterns, and atomic resolution images. To obtain the thinnest possible specimens for very high-resolution imaging, wedge-shaped lamellae were produced.

STEM images were taken with a double-corrected JEOL ARM 200F TEM/STEM operating at 200 kV, with a beam convergence semi-angle of 22 mrad. The annular bright field (ABF) and annular dark field (ADF) detectors covered 11.5-24 and approximately 45-180 mrad, respectively[11]. In atomic resolution STEM images, atom positions are determined by fitting two-dimensional Gaussian peaks[11,20].

EELS data and ADF images were acquired at the UK SuperSTEM Laboratory using a Nion UltraSTEM 100 MC operated at 60 kV, with a beam convergence semi-angle of 32 mrad. The acceptance semi-angles of EELS and ADF were 44 mrad and 79-185 mrad, respectively.

RESULTS AND DISCUSSION

Domains on the polished (001) surface imaged by PFM follow a regular stripe pattern running along [$\bar{1}$10] with reversal of both in-plane and out-of-plane phase and alternating sawtooth and straight domain walls, as shown in Figure 1A and Supplementary Figure 1A. No relation between domain structure and surface topography was present (see Supplementary Figure 1B). The spacing between stripes varies between 60 and 120 nm. Occasionally, domains can be found to terminate where sawtooth and straight domain walls meet (e.g., at x in Figure 1), indicating that these two types of walls separate the sample into only two different domains. Bright-field (BF) STEM images of (110) and (010) FIB lift-out lamellae are shown in Figure 1B and C (see Supplementary Figure 2A). In both (110) and (010) orientations, the domain walls appear as alternating sawtooth and planar bands of contrast. In these BF-STEM images, the crystal is

aligned to the zone axis, and local conditions, such as strain, composition, or a small change in crystal orientation across a boundary, can strongly affect the transmission of the electron probe. As a result, domain boundaries appear slightly darker. Their orientation varies depending on the direction of view. In the (110) section [Figure 1B], straight bands are parallel to the (001) surface, while in the (010) section [Figure 1C], they are inclined at an angle of approximately 25°, running along [$\bar{2}$01]. Sawtooth walls present different V-shapes when observed from different directions, and their structure is considered in detail elsewhere[19]. The domain appearance and PFM measurements agree with the observations of Berger *et al.*[16]. However, they interpreted the flat bands of contrast seen in Figure 1B and C as domains with a width of approximately 10 nm. The varying thickness of the lamellae in Figure 1 shows this to be incorrect. In Figure 1C, the lamella decreases to a thickness of just a few nm at the edge of the specimen on the top-right of the image. The width of the bands decreases as the specimen thickness decreases, indicating that they correspond to planes in the material that are inclined to the direction of view. The same effect can also be seen in Figure 1B, where the specimen thickness increases towards the bottom of the image. Therefore, the darker bands are not slabs of material that form domains, different to the adjacent lighter material. They are the projection of a plane that is inclined to the point of view.

The proposal that the flat bands of contrast in Figure 1B and C are planes rather than slabs of finite thickness is confirmed by the ($\bar{1}$10) section shown in Figure 2A. In this projection, their width does not depend on specimen thickness. Here, they are seen edge-on and appear as sharp, straight lines at an angle of 35° to (001) surface, i.e., lying on (112) planes. The sawtooth domain pattern can be recognised in the thinnest part of the specimen but becomes indistinct where the lamella is thicker due to overlapping projections. Higher magnification images [Supplementary Figure 2B] show that the average habit plane is slightly away from (112); the flat domain walls have a terraced structure, with (112) facets seen edge-on, separated by steps 1-2 nm in height.

High-resolution ($\bar{1}$10) STEM images of one of these domain walls, seen edge-on in the thinnest part of the specimen, are shown in Figure 2C and D. In any {110} section of BiFeO$_3$, the [111] polar axis can either lie within the plane of the section or at 35° to it, (i.e. with an out-of-plane component). The $a^-a^-a^-$ antiphase tilting of oxygen octahedra in the *R3c* structure gives different projections for the two cases. When the polar axis is in the image plane, the antiphase tilting of octahedra is not visible, and oxygen columns appear as a dumbbell at the same location in every unit cell[21]. Conversely, when it has an out-of-plane component, O-Fe-O-Fe-O chains form an arc with a curvature indicating the direction of $\mathbf{P}_s$[17] [Supplementary Figure 3]. In Figure 2C, the polar axis is in the image plane for both domains, consistent with a [$\bar{1}$10] BiFeO$_3$ projection [Figure 2B]. On a unit-cell level, polarisation $\mathbf{P}_s$ is often taken to be proportional to the negative displacement of Fe relative to the centre of the rectangle defined by its four Bi neighbours, namely -$\boldsymbol{\delta}_{FB}$[22,23]. Since the polar axis lies in the image plane, we observe a full projection of the displacement (in comparison, one can only observe approximately 57% or 81% of the displacement in [110] or [100] projections, respectively[23]). The quiver map of -$\boldsymbol{\delta}_{FB}$ vectors overlaid on the ADF-STEM image of Figure 2D shows that polarisation changes by 180°, pointing towards the wall on both sides. (N.B. at the domain wall itself, $\boldsymbol{\delta}_{FB}$ is not calculated because it is unclear how to define the unit cell.) Away from the domain wall, the magnitude of $\boldsymbol{\delta}_{FB}$ is generally around 40 pm, in good agreement with the theoretical value of 41 pm for P_s of approximately 100 μC cm^{-2}[7,23,24]. As a final observation in Figure 2D, Bi atom columns in the domain wall are not as bright as equivalent atom columns in the surrounding material, indicating a lower occupancy of Bi at the domain wall.
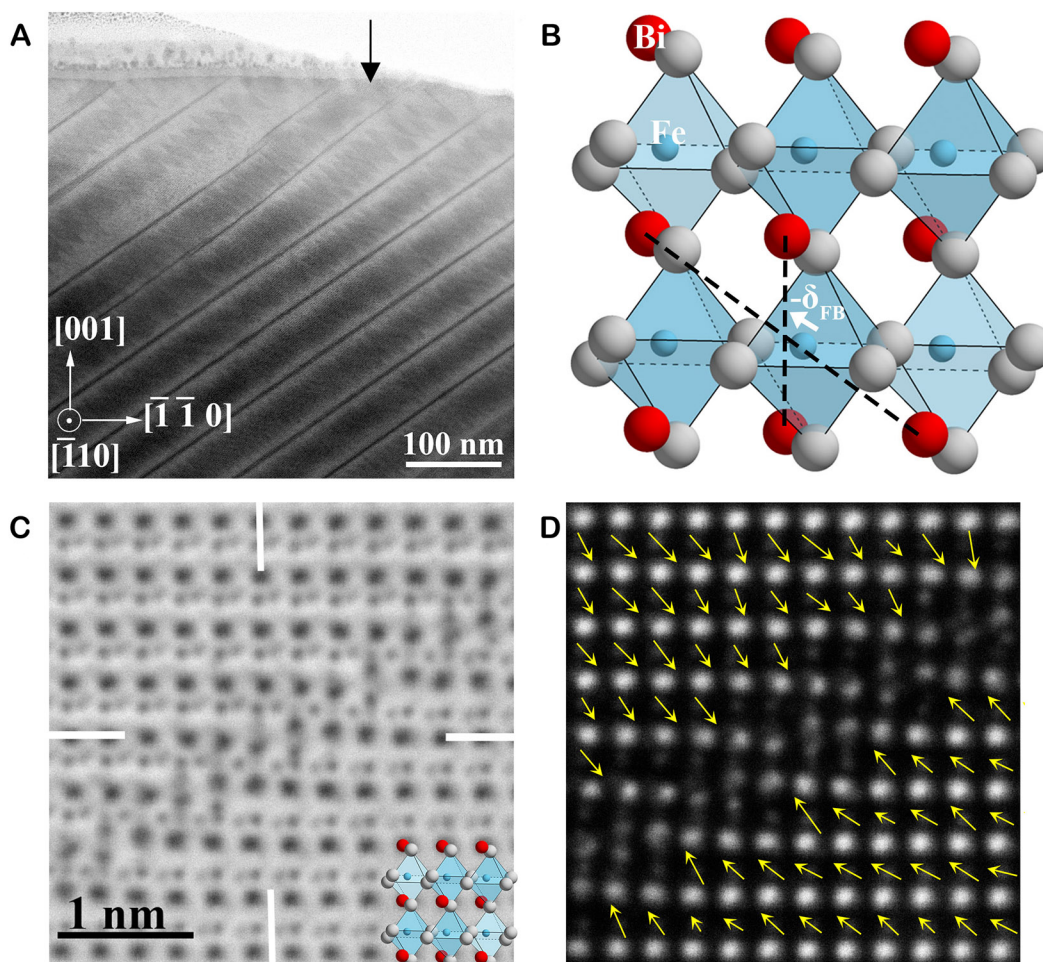
Figure 2. (A) Low magnification BF-STEM image of a $(\bar{1}10)$ FIB-prepared lamella. The dark arrow at the thin edge of the lamella points towards increasing thickness. The width of the straight dark lines is independent of specimen thickness, showing that they correspond to planes seen edge-on. The crystal orientation applies to all images in this figure. (B) Ideal $(\bar{1}10)$ projection of $BiFeO_3$, where Bi atoms are presented in red, Fe blue, and O grey. The direction of the $-\boldsymbol{\delta}_{FB}$ vector is also shown. (C) A high-resolution ABF-STEM image of a flat wall. White lines are aligned horizontally and vertically, allowing the rigid-body displacement of the domains along [110] and [001] to be seen. (D) An ADF-STEM image taken simultaneously with C). Arrows in (D) show local $-\boldsymbol{\delta}_{FB}$ vectors, indicating the magnitude and direction of polarisation in each unit cell.

It is apparent from Figure 2C and D that these 180° head-to-head domain walls are reconstructed; the local structure is different from the bulk crystal, and the associated distortions are quantified in Figure 3. Examining the horizontal (001) planes of bright Bi atom columns in Figure 2D, downwards displacements (i.e., along $[00\bar{1}]$) are seen on the left, starting approximately 0.5 nm away from the domain wall, while upwards displacements along [001] are seen on the right. These displacements are shown as blue points and lines in Figure 3A and reach a value of approximately 0.1 nm at the domain wall itself. Far from the domain wall, these displacements tend to zero, showing that the (001) planes are aligned, as can be directly seen from the horizontal white lines in Figure 2C. The orange line in Figure 3A shows a similar measurement for the vertical (110) planes. Here, there is greater scatter as the displacements vary from place to place along the domain wall. Interestingly, there is a slight increase in displacements immediately adjacent to the domain wall. Additionally, a long-range misalignment of about 0.1 nm is observed, corresponding to a lateral shift of ½[110]. This rigid-body displacement can be directly observed in Figure 2C by comparison of the vertical white lines with the position of atom columns. The average value of P_s changes its sign abruptly
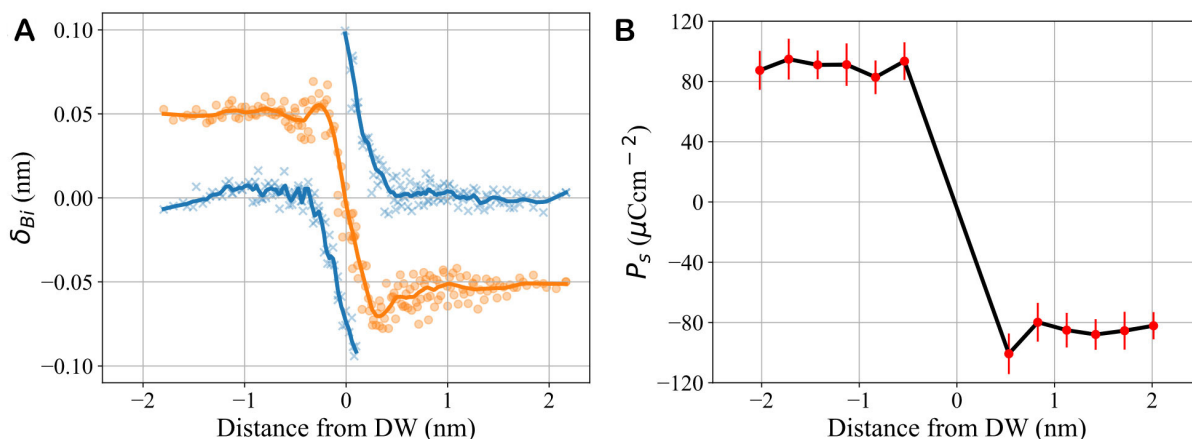
Figure 3. (A) Distortion of unit cells in the vicinity of the domain wall shown in Figure 2D, measured by the displacement of Bi atom columns away from (110) planes (orange) or (001) planes (blue). Points correspond to individual measurements, and the line is an average value. (B) Average polarisation P_s obtained from -δ_{FB} vectors, measured in bands parallel to the domain wall.

(over approximately 1 nm) at the wall [Figure 3B], which is significantly different from the previously reported thicker (> 2 nm) widths for charged domain walls in $BiFeO_3$ without any local reconstruction[23,25-27]. The narrow domain wall width indicates the presence of a strong electrical field related to the local change in structure at the domain wall.

More information on the reconstruction at these domain walls can be obtained from a second point of view, obtained from a (010) section shown in Figure 4. Although the domain wall is probably inclined to the electron beam direction, this image is taken at the thinnest part of the lamella, and the high electron beam convergence angle gives a reduced depth of field[28]. Consequently, the domain wall is sharply delineated in ADF-STEM images. (The effect of reduced depth of field is shown in Supplementary Figure 4). At the domain wall [Figure 4A], the reconstruction appears as alternating bright and dark clusters of atoms, forming either 2 × 1 or 2 × 2 atom blocks, while -δ_{FB} vectors demonstrate the 180° head-to-head nature [Figure 4B]. There is no obvious change in the magnitude of P_s immediately adjacent to the reconstructed domain wall, which is approximately 1.5 unit cells in width and runs along $[\overline{2}01]$ in this projection. Just as in the $[\overline{1}10]$ images of Figure 2, (001) planes are fully aligned (horizontal white lines), while a ½[100] displacement is visible (vertical white lines). Since the component along the beam direction is not visible, this is in full agreement with the ½[110] rigid body shift observed in Figure 2. Bending of the (001) Bi planes can also be found at the domain wall (see Supplementary Figure 5). Figures 4E-G show core-loss EELS elemental maps of the domain wall, together with a simultaneously recorded ADF image in Figure 4D. The brightest atom columns in the ADF image are shown to be Bi in a separate EELS acquisition [Supplementary Figure 6]. Dark regions in the ADF image at the domain wall lack Bi and consist of Fe+O. These findings, along with the results presented in Figures 2 and 4, show that the flat domain wall has a structure and stoichiometry different from bulk $BiFeO_3$. They are consistent with each other both in the observed rigid-body shift, lower Bi content, bending of (001) Bi planes, and P_s distribution around them.

The nonstoichiometry of the reconstruction in the flat 180° head-to-head walls is an indication that they form during crystal growth, while the periodic domain structure indicates a degree of self-organisation. Synthesis of crystalline $BiFeO_3$ is only possible within a narrow range of conditions, both in the deposition of thin epitaxial layers[22,29-32] and as ceramics or single crystals[31,33-35]. In bulk crystal growth, the secondary Bi-rich sillenite $Bi_{25}FeO_{39}$ and/or Fe-rich mullite $Bi_2Fe_4O_9$ phases readily form to accommodate deviations
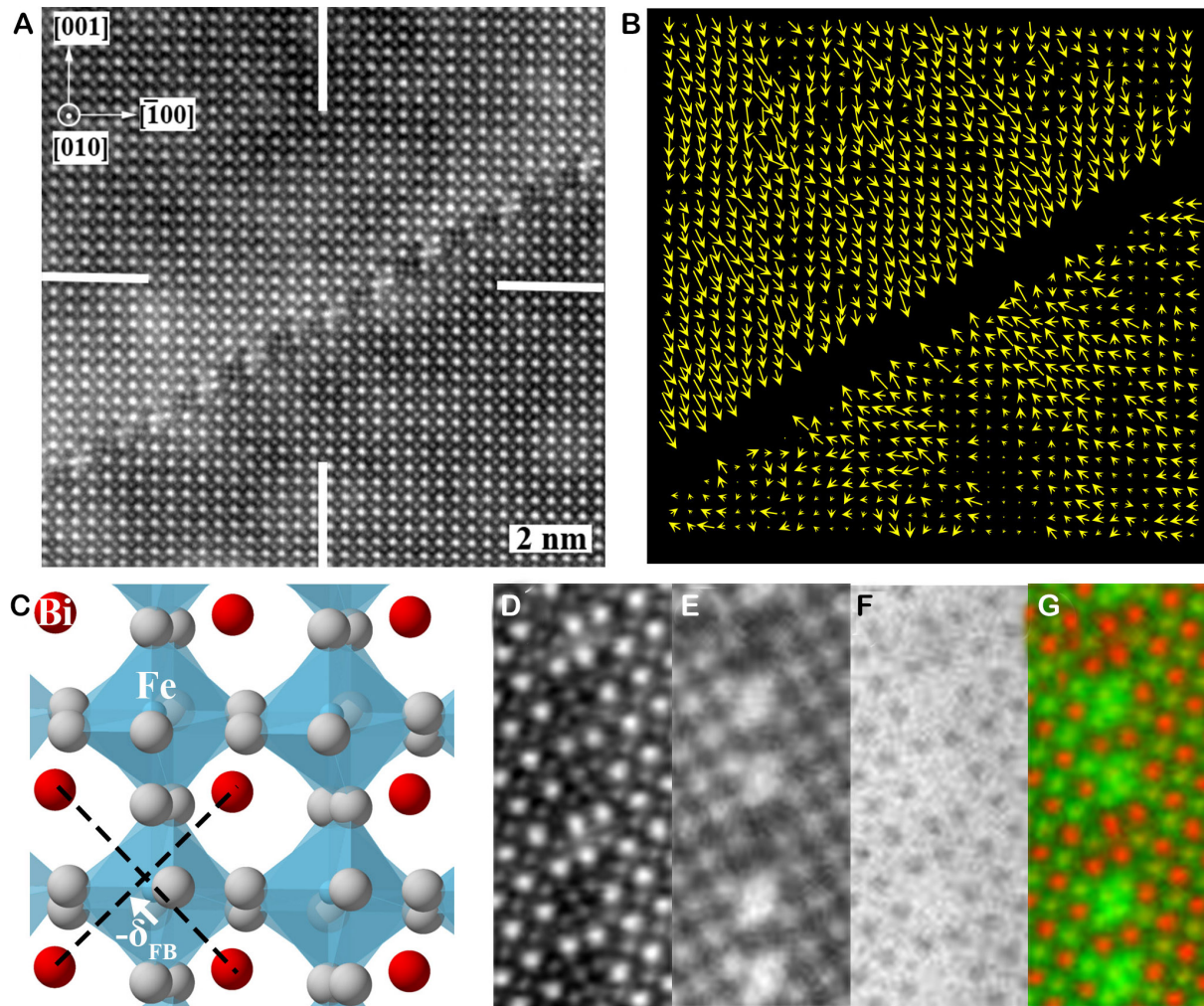
Figure 4. (A) An ADF-STEM image of a head-to-head 180° domain wall in a (010) FIB-prepared lamella. Large and bright atoms columns are Bi, and smaller ones are Fe. O atoms are not visible. (B) Quiver plot of local $-\delta_{FB}$ vectors, indicating the magnitude and direction of polarisation in each unit cell. (C) Ideal (010) projection of $BiFeO_3$; Bi atoms are red, Fe blue, and O grey. The direction of the $-\delta_{FB}$ vector is also shown. (D-G) core-loss EELS data: image size is 1.32 × 3.13 nm. (D) HAADF-STEM; (E) an element map of Fe; (F) an element map of O; (G) a composite of ADF (red) and Fe (green).

from perfect stoichiometry, e.g., due to the relative volatility of Bi_2O_3[33,35]. In epitaxial thin film growth, locally nonstoichiometric planar defects that strongly resemble those shown in Figure 4 are often seen[22,29,30,32,36,37]. Maclaren *et al.* found iron-rich regions consisting of edge-sharing FeO_6 octahedra, resembling the structure of γ-Fe_2O_3, (and, indeed, mullite)[30,36,37]. Li *et al.* showed that they can be induced by a slight increase in substrate temperature during MBE deposition, which makes the surface Fe-rich[22,29,32]. Similar to the observed reconstruction in this study, these previously observed planar defects also have a half-unit-cell rigid body shift across them caused by the switch from corner-sharing to edge-sharing oxygen octahedra. The deviation from stoichiometry gives a local excess of oxygen anions, giving a negative charge density estimated to be between -68 μC cm^{-2} and -110 μC cm^{-2}[22,36,37]. The effect of these negatively charged planar defects in the surrounding $BiFeO_3$ matrix is to induce an increased local polarisation towards them, producing charged head-to-head domain walls[32]. The intrinsic negative charge density accommodates the majority of the -190 μC cm^{-2} polar discontinuity expected at the flat domain walls in our crystal, explaining the relatively narrow region of adjacent material that has a different polarisation to the bulk material.

Therefore, in our material, we may explain the origin of the domain microstructure as follows. Since the temperature during crystal growth is below T_c, ferroelectric domains are to be expected, and ideally, they would assume a form to minimise the competing ferroelectric/ferroelastic/electrostatic energy components of the system. In thin film growth, it is well established that domain microstructures may evolve during film deposition[38] and, in turn, can influence growth morphology[39]. Therefore, in our case of single-crystal BiFeO₃ growth, we may expect regions with positive and negative surface charges that have an effect on domain structure and subsequent growth. Importantly, Li[29] showed that nonstoichiometric monolayers may form on polarisation-up, negatively charged BiFeO₃ growth surfaces. They found that as growth progresses, a region with polarisation pointing towards the growth surface may, therefore, reach a critical negative charge, causing the incorporation of FeO_6 octahedra at the crystal surface and producing nonstoichiometric monolayers of the defective material. They also showed that the negative charge induces and pins head-to-head polarisation[32]. It seems plausible that a similar mechanism is responsible for the head-to-head domain walls that we observe. On a (*hhl*) growth surface, the FeO_6 octahedra would form edge-sharing chains along $[1\bar{1}0]$, partly defining the orientation of the wall. These negatively-charged defects stabilise the 180° domain walls and perpetuate incorporation of FeO_6 octahedra in the next monolayer of crystal growth. It is not clear if the (112) plane makes the best match of their structure to the adjacent *R3c* BFO or whether this habit plane is a result of the asymmetrical surface charge where the domain wall intersects the surface, which may vary with, for example, the growth rate. An array of such structures can only exist with a further reversal of polarisation between them, and tail-to-tail 180° domain walls are the most efficient way of achieving this. The presence of the sawtooth walls is thus topologically necessary. It has been shown that unpinned 180° domain walls are expected to develop a crenellated structure to balance polarisation and electrostatic energy[40,41]. The crenellated structure of these walls indicates that they are not pinned in the same way as the flat walls, and a very recent study of these tail-to-tail walls indicates that they are, to some extent, mobile when an electric field is applied, while head-to-head flat walls are immobile[18]. This is in good agreement with our measurements of P_s hysteresis, which gave essentially no signal, indicating that the flat walls are completely pinned. It is commonly observed that measurements of P_s in bulk BiFeO₃ crystals are usually an order of magnitude smaller than in thin films, even though our measured $\boldsymbol{\delta}_{FB}$ vectors at the atomic scale are similar, equivalent to P_s approximately 100 μC cm^{-2}. While this batch of material now dominates high-resolution structural studies of bulk BiFeO₃[16,17], there is nothing in the proposed origin of the domain structure that would indicate it to be specific to these particular crystals. On a macroscopic scale, the deviation from perfect stoichiometry is miniscule; approximating the defects as sheets of Bi with 50% occupancy, a spacing of 100 nm gives a Fe excess of only approximately 0.2 at.%, meaning that they are unlikely to be avoided by changes in starting composition.

CONCLUSIONS

Periodic domain structures in single crystal BiFeO₃ have been re-investigated. Our results show that all domain walls are of 180°-type, alternating between flat head-to-head and sawtooth tail-to-tail walls. We focus on the flat walls here, finding that they have an orientation close to (112) and a polarisation reversal that occurs over only approximately 1 nm, significantly less than seen in other charged domain walls in BiFeO₃. They are locally nonstoichiometric, with an atomic reconstruction of roughly a unit cell in thickness, similar to that seen in planar defects in thin film BiFeO₃ and related materials. The reconstructed region contains edge-sharing FeO_6 octahedra that produce a rigid-body shift of half a unit cell and a negative charge density that induces head-to-head polarisation. We propose that the periodic domain structure forms during crystal growth in regions where negative surface charges exceed a critical value, causing the incorporation of FeO_6 octahedra that is perpetuated and becomes self-organised as growth proceeds. The reconstruction and local charge strongly pin head-to-head 180° domain walls, explaining the poor response of these BiFeO₃ single crystals in measurements of polarisation. Avoiding their formation is,

therefore, a necessary prerequisite for high-performance $BiFeO_3$ crystals and ceramics.

DECLARATIONS

Authors' contributions

Performed data acquisition, data analysis, and interpretation and wrote the first draft of the article: Ge W, Sanchez AM

Performed data acquisition (STEM+EELS maps) at SuperSTEM: Ramasse Q

Provided material, conception and design of the study and interpretation: Alexe M

Performed data analysis and interpretation and contributed to the development of the article: Beanland R, Sanchez AM

AVAILABILITY OF DATA AND MATERIALS

The data that support the findings of this study are openly available in WRAP at http://wrap.warwick.ac.uk/173964.

Conflicts of interest

All authors declare that there are no conflicts of interest.

Ethical approval and consent to participate

Not applicable.

Consent for publication

Not applicable.

REFERENCES

1. Neaton JB, Ederer C, Waghmare UV, Spaldin N, Rabe K. First-principles study of spontaneous polarization in multiferroic $BiFeO_3$. *Phys Rev B* 2005;71:014113. DOI
2. Ramesh R, Spaldin NA. Multiferroics: progress and prospects in thin films. *Nat Mater* 2007;6:21-9. DOI PubMed
3. Wang J, Neaton JB, Zheng H, et al. Epitaxial $BiFeO_3$ multiferroic thin film heterostructures. *Science* 2003;299:1719-22. DOI
4. Catalan G, Scott JF. Physics and applications of bismuth ferrite. *Adv Mater* 2009;21:2463-85. DOI
5. Eerenstein W, Mathur ND, Scott JF. Multiferroic and magnetoelectric materials. *Nature* 2006;442:759-65. DOI PubMed
6. Scott JF. Data storage. Multiferroic memories. *Nat Mater* 2007;6:256-7. DOI
7. Kubel F, Schmid H. Structure of a ferroelectric and ferroelastic monodomain crystal of the perovskite $BiFeO_3$. *Acta Crystallogr B Struct Sci* 1990;46:698-702. DOI
8. Glazer AM. The classification of tilted octahedra in perovskites. *Acta Crystallogr B Struct Crystallogr Cryst Chem* 1972;28:3384-92. DOI
9. Catalan G, Seidel J, Ramesh R, Scott JF. Domain wall nanoelectronics. *Rev Mod Phys* 2012;84:119-56. DOI
10. Yadav AK, Nelson CT, Hsu SL, et al. Observation of polar vortices in oxide superlattices. *Nature* 2016;530:198-201. DOI
11. Peters JJP, Apachitei G, Beanland R, Alexe M, Sanchez AM. Polarization curling and flux closures in multiferroic tunnel junctions. *Nat Commun* 2016;7:13484. DOI PubMed PMC
12. Rusu D, Peters JJP, Hase TPA, et al. Ferroelectric incommensurate spin crystals. *Nature* 2022;602:240-4. DOI
13. Meyer B, Vanderbilt D. *Ab* initio study of ferroelectric domain walls in $PbTiO_3$. *Phys Rev B* 2002;65:104111. DOI
14. Bhatnagar A, Roy Chaudhuri A, Heon Kim Y, Hesse D, Alexe M. Role of domain walls in the abnormal photovoltaic effect in $BiFeO_3$. *Nat Commun* 2013;4:3835. DOI PMC

15.   Seidel J, Martin LW, He Q, et al. Conduction at domain walls in oxide multiferroics. *Nat Mater* 2009;8:229-34. DOI

16.   Berger A, Hesse D, Hähnel A, Arredondo M, Alexe M. Regular nanodomain vertex arrays in BiFeO$_3$ single crystals. *Phys Rev B* 2012;85:064104. DOI

17.   Jia C, Jin L, Wang D, et al. Nanodomains and nanometer-scale disorder in multiferroic bismuth ferrite single crystals. *Acta Mater* 2015;82:356-68. DOI

18.   Condurache O, Dražić G, Rojac T, et al. Atomic-level response of the domain walls in bismuth ferrite in a subcoercive-field regime. *Nano Lett* 2023;23:750-6. DOI PubMed PMC

19.   Ge W, Beanland R, Alexe M, Sanchez AM. 3D reconstruction of sawtooth 180° tail-to-tail domain walls in single crystal BiFeO$_3$. *Adv Funct Mater* 2023:2301171. DOI

20.   Peters JJP, Bristowe NC, Rusu D, et al. Polarization screening mechanisms at La$_{0.7}$Sr$_{0.3}$MnO$_3$-PbTiO$_3$ interfaces. *ACS Appl Mater Interfaces* 2020;12:10657-63. DOI

21.   Woodward DI, Reaney IM. Electron diffraction of tilted perovskites. *Acta Crystallogr B* 2005;61:387-99. DOI PubMed

22.   Li L, Zhang Y, Xie L, et al. Atomic-scale mechanisms of defect-induced retention failure in ferroelectrics. *Nano Lett* 2017;17:3556-62. DOI

23.   Nelson CT, Winchester B, Zhang Y, et al. Spontaneous vortex nanodomain arrays at ferroelectric heterointerfaces. *Nano Lett* 2011;11:828-34. DOI

24.   Lebeugle D, Colson D, Forget A, Viret M. Very large spontaneous electric polarization in BiFeO$_3$ single crystals at room temperature and its evolution under cycling fields. *Appl Phys Lett* 2007;91:022907. DOI

25.   Condurache O, Dražić G, Sakamoto N, Rojac T, Benčan A. Atomically resolved structure of step-like uncharged and charged domain walls in polycrystalline BiFeO$_3$. *J Appl Phys* 2021;129:054102. DOI

26.   Bednyakov PS, Sturman BI, Sluka T, Tagantsev AK, Yudin PV. Physics and applications of charged domain walls. *NPJ Comput Mater* 2018;4:65. DOI

27.   Li L, Gao P, Nelson CT, et al. Atomic scale structure changes induced by charged domain walls in ferroelectric materials. *Nano Lett* 2013;13:5218-23. DOI

28.   Nellist PD, Pennycook SJ. The principles and interpretation of annular dark-field Z-contrast imaging. *Adv Electron Electron Phys* 2000;113:147-203. DOI

29.   Li L, Jokisaari JR, Zhang Y, et al. Control of domain structures in multiferroic thin films through defect engineering. *Adv Mater* 2018;30:e1802737. DOI

30.   MacLaren I, Sala B, Andersson SM, et al. Strain localization in thin films of Bi(Fe,Mn)O$_3$ due to the formation of stepped Mn^{4+}-rich antiphase boundaries. *Nanoscale Res Lett* 2015;10:407. DOI PubMed PMC

31.   Deniz H, Bhatnagar A, Pippel E, et al. Nanoscale Bi$_2$FeO$_{6-x}$ precipitates in BiFeO$_3$ thin films: a metastable Aurivillius phase. *J Mater Sci* 2014;49:6952-60. DOI

32.   Li L, Cheng X, Jokisaari JR, et al. Defect-induced hedgehog polarization states in multiferroics. *Phys Rev Lett* 2018;120:137602. DOI

33.   Rojac T, Bencan A, Malic B, et al. BiFeO$_3$ ceramics: processing, electrical, and electromechanical properties. *J Am Ceram Soc* 2014;97:1993-2011. DOI

34.   Wu J, Fan Z, Xiao D, Zhu J, Wang J. Multiferroic bismuth ferrite-based materials for multifunctional applications: Ceramic bulks, thin films and nanostructures. *Prog Mater Sci* 2016;84:335-402. DOI

35.   Lu J, Qiao L, Fu P, Wu Y. Phase equilibrium of Bi$_2$O$_3$-Fe$_2$O$_3$ pseudo-binary system and growth of BiFeO$_3$ single crystal. *J Cryst Growth* 2011;318:936-41. DOI

36.   Maclaren I, Wang L, Craven AJ, et al. The atomic structure and chemistry of Fe-rich steps on antiphase boundaries in Ti-doped Bi$_{0.9}$Nd$_{0.15}$FeO$_3$. *APL Mater* 2014;2:066106. DOI

37.   Maclaren I, Wang L, Morris O, et al. Local stabilisation of polar order at charged antiphase boundaries in antiferroelectric (Bi$_{0.85}$Nd$_{0.15}$)(Ti$_{0.1}$Fe$_{0.9}$)O$_3$. *APL Mater* 2013;1:021102. DOI

38.   Luca G, Strkalj N, Manz S, Bouillet C, Fiebig M, Trassin M. Nanoscale design of polarization in ultrathin ferroelectric heterostructures. *Nat Commun* 2017;8:1419. DOI PubMed PMC

39.   Wang H, Wu H, Chi X, et al. Large-scale epitaxial growth of ultralong stripe BiFeO$_3$ films and anisotropic optical properties. *ACS Appl Mater Interfaces* 2022;14:8557-64. DOI

40.   Zhang J, Wang Y, Liu J, et al. Origin of sawtooth domain walls in ferroelectrics. *Phys Rev B* 2020;101:060103. DOI

41.   Marton P, Gonçalves MAP, Paściak M, et al. Zigzag charged domain walls in ferroelectric PbTiO$_3$. *Phys Rev B* 2023;107:094102. DOI